SECOND EUROPEAN CONFERENCE ON EARTHQUAKE ENGINEERING
AND SEISMOLOGY, ISTANBUL AUG. 25-29, 2014

EVALUATION OF SEISMIC PERFORMANCE OF SLENDER L-SHAPED AND T-SHAPED RC STRUCTURAL WALLS

Zhong Wen ZHANG[1] and Bing LI[2]*

ABSTRACT

L and T-shaped slender reinforced concrete (RC) structural walls are commonly used in medium-rise and high-rise buildings as part of the lateral force resisting system. Despite being a commonly utilized member in structures around the world, experimental results on seismic performance of these walls are limited, especially that regarding behavior of the non-rectangular RC walls in non-principal bending directions. This paper aims to provide additional experimental evidence on the seismic performance of non-rectangular RC structural walls. Experimental results for two L-shaped and two T-shaped RC walls tested in different loading directions were presented. The experimental results were compared with analytical results from nonlinear fibre models and 3-dimensional finite element models. Performances of these walls were analyzed and main conclusions were summarized in this paper.

INTRODUCTION

Slender structural walls characterized by flexure dominated behaviour are one of the most common elements in RC buildings and these sections can come in a variety of shapes. In recent years, research has demonstrated that some issues vital to seismic performance of these walls remain insufficiently addressed, including the shear lag effect [Hassan and El-Tawil 2003], deformation component and behaviour of the wall in multiple loading directions [Thomsen Iv and Wallace 2004; Beyer, Dazio et al. 2008; Brueggen 2009]. Compared to rectangular RC walls, experimental data regarding these walls are limited, and most are derived from specimens designed with good ductility. For non-rectangular walls with inferior detailing commonly found in conventional structures, their vulnerability to possible earthquake loading remains unclear.

This research aims to provide a better understanding of the behaviour of non-rectangular RC walls especially those with inferior detailing, thus contributing to evaluating of existing buildings and development of design guidelines for non-rectangular walls in regions with low or moderate seismic hazard.

Experimental Program

Drawings of the specimens are shown in Figure 1. The wall geometries, details and materials were selected to resemble structural walls found in existing buildings in Singapore. These specimens were designed for moderate ductility and differed from walls designed for good ductility in four main aspects. Firstly, the longitudinal reinforcement ratio of the specimens was higher. Secondly, the target

[1] Ph. D. candidate, Nanyang Technological University, Singapore, chuangwendell@gmail.com
[2]* Presenter and corresponding author, Associate professor, Nanyang Technological University, Singapore, cbli@ntu.edu.sg

ductility factor (DF) assumed was as 3 in determining the requirements for confined boundary elements, which was relatively low. Thirdly, some requirements from ACI318-08 and EC8 on spacing of the transverse reinforcement at boundary elements of the wall were not met. Fourth, shear demands of some specimens imposed by the lateral reaction force were larger than the shear resistance given by the specific requirements for seismic design in ACI318-08 and EC8, as shown in Table 2. In calculation of the shear demand, the shear force was assumed to be carried only by the wall segment in compression. The shear demand and capacity for both the web and the half of the flange in compression were calculated for specimen TWN.

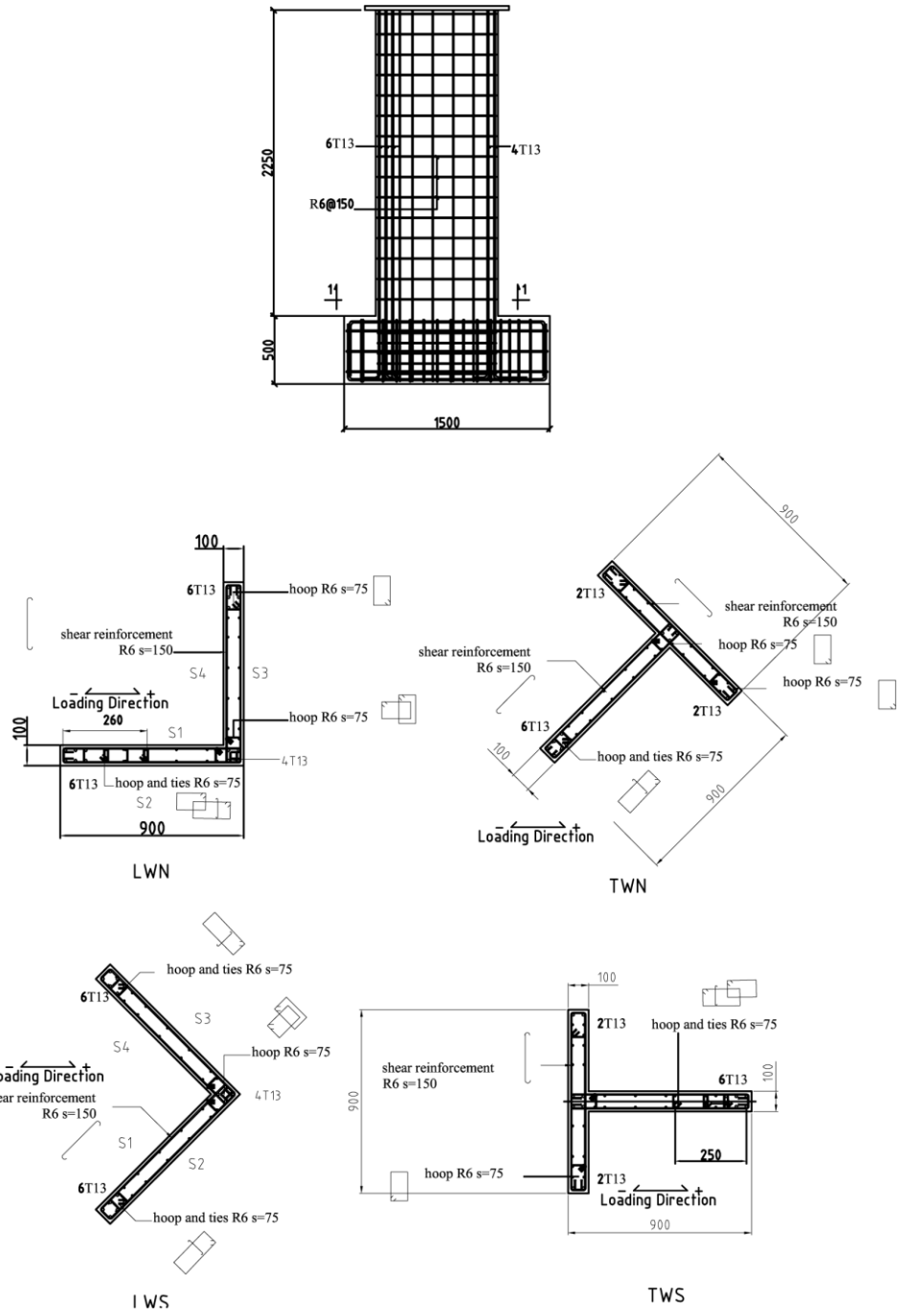

Figure 1. Detailing of the specimens

Table 1. Summary of Test Specimens

Specimen	Section	H	P	A_s	s	f'_c

	$l_w x l_w x t$	(mm)	$f'_c A_g$	(mm^2)	(mm)	(MPa)
LWS	900x900x100	2250	0.10	2835.2	150	29.8
LWN			0.10	2835.2	150	29.2
TWS			0.10	2705.1	150	27.5
TWN			0.10	2705.1	150	32.4

Table 2. Shear Demand and Shear Capacity of Specimens

Specimen	Expected shear force	ACI318-05			Diagonal compression capacity	
		Shear strength	Shear strength limits for crack control	Shear strength for earthquake resistance	EC8	Paulay and Priestley
LWS	223	308.0	748.4	266.3	297.0	292.1
LWN	314	308.0	748.4	266.3	297.0	292.1
TWS	331	308.0	748.4	266.3	297.0	292.1
TWN web	163	308.0	748.4	266.3	297.0	292.1
TWN half flange	108	142.8	332.6	118.4	132.0	129.8

The test specimens were attached to a loading apparatus enabling the specimens to deform under single curvature bending. Cyclic lateral loads were applied at top of the specimens together with a constant axial load. Specifically, two lateral braces with load cells perpendicular to the loading plane were installed to restrain the out-of-plane deformation and to measure the out-of-plane reactions. The specimens went two cycles for each lateral load level before the lateral load increased to the next level. The first eight cycles were force-controlled with limits of 25, 50, 75, and 100% of the predicted lateral forces at first yield. The cycles afterward were displacement controlled according to the ductility factor.

Figure 2. Experimental setup

Analytical Program

The prediction of the force-displacement relationship is a vital process in displacement-based design. As slender RC walls are characterized by flexural behaviour, such a relationship can be predicted by analyses on critical sections of the walls together with plastic hinge analyses. Sectional analyses are performed to establish the moment-curvature relationships for the critical sections. Plastic hinge analyses are then conducted to convert the curvature of the critical sections to the top displacements of the walls. In this research project, nonlinear section analyses were performed in the Engineers' Studio program with fibre element approach. Specifically, stress-strain curves of the plain and confined concrete were modelled explicitly. The plastic hinge length was estimated by the equations proposed by Paulay and Priestley:

$$L_{ph} = 0.08h + 0.022 d_b f_y$$
$$L_{ph} = 0.2 l_w + 0.044h \quad (1)$$

in which h is the wall height, d_b is the diameter of the main longitudinal reinforcement bar, f_y is the yield strength in MPa, and l_w is the wall length parallel to the loading direction. Predictions of the force-displacement relationships for different specimens were summarized in Figure 4 together with the experimental hysteresis loops.

Apart from the plastic hinge analyses, three-dimensional finite element models were built regarding the specimens. These models have been developed in the DIANA 9.1 (Displacement method Analyser, version 9.1) program. In these models, the concrete was modelled with 20 point isoparameteric solid elements, while the vertical, horizontal and transverse reinforcement was modelled embedded into the concrete elements. Meshing of the model was demonstrated in Figure 3. The mesh was fine in bottom of the model to capture the dramatic variation of strain in this region and coarser as the height increased. For reinforcement bars, an elasto-plastic material model with strain hardening by employing the Von Mises yield criterion was assumed. The concrete, on the other hand, followed the Modified Compression Field Theory by Vecchio and Collins which simulates behaviour of the concrete in a smeared fixed crack approach.

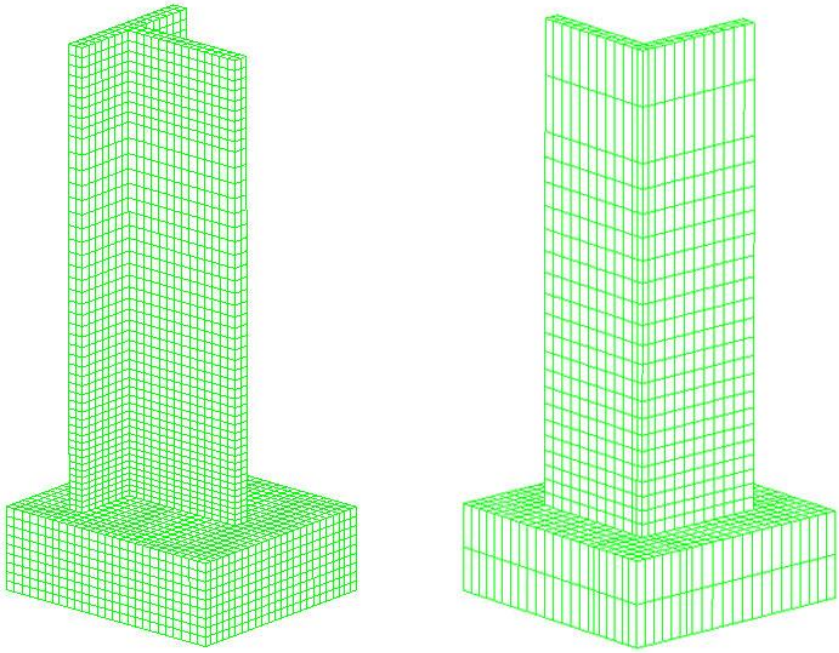

Figure 3. Meshing of the FE models

Test Results

Hysteretic responses of test specimens were presented in Figure 4. The test-derived hysteretic responses were compared with the backbone curves predicted by plastic hinge analyses and FE analyses as described in previous section. The plastic hinge analyes generally overestimated stiffness of the specimens. For TWN and LWS, maximum lateral load predicted by the plastic hinge analyses were reached in the test. For TWS and LWN, the test-derived maximum lateral reaction did not reach the estimation made by plastic hinge analyses. The estimated backbone curves made by FE analyses, on the other hand, agreed with the test derived hysteresis loops well in all these specimens. Omission of the shear lag effect and the shear deformation in the plastic hinge analyses was believed to be responsible for the overestimation of the force and the stiffness of the specimens. Further discussions will be given later on with data of the strain in vertical reinforcement and deformation compositions.

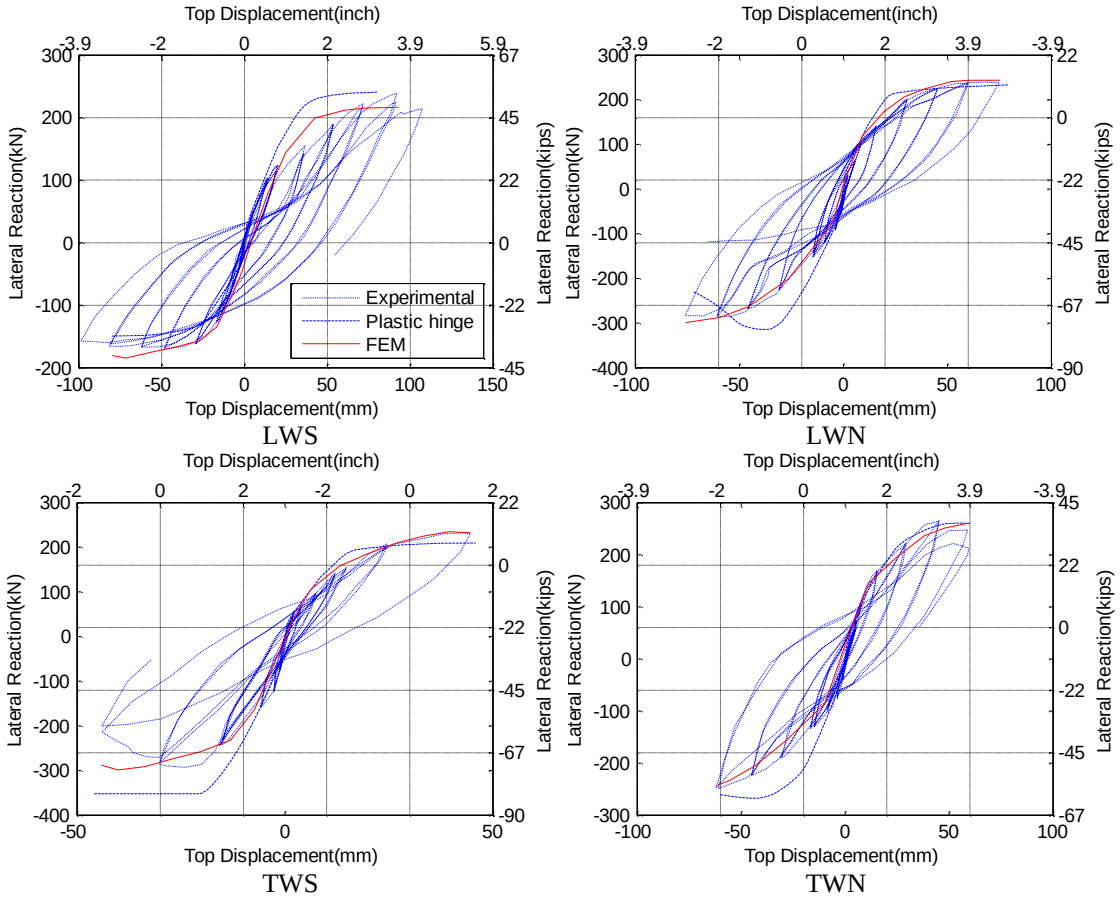

Figure 4. Experimental and predicted deformation-reaction curves

Three kinds of failure mechanism were identified for the tested specimens. The first failure mechanism was only observed in specimen LWS. The specimen failed due to crushing of concrete in the confined wall tip, as shown in Figure 5. Concrete spalling was observed in cycles with DF = 4 in the specimen, together with buckling of some longitudinal reinforcement bars. However, the well confined concrete in the boundary elements prevented the wall from losing significant lateral load capacity. As larger top displacement imposed higher compression strain in the specimen, concrete at boundary elements finally crushed. The wall failed correspondingly. The second failure mechanism was observed in LWN and TWN. Concrete spalling and buckling of longitudinal bars were also observed in these walls before this failure mechanism occurred. However, significant loss of lateral load capacity was a consequence of loss of stability of the wall segment in compression. For LWN, it was tip of the wall web. For TWN, it was the outer half of the flange. It was observed during that test that the wall segment in compression would deflect slightly in the out-of-plane direction while it was in compression. As the wall segment was carrying a large compression force, this deflection introduced significant moment in the plane perpendicular to the loading plane, which, in turn, introduced larger deflection in the out-of-plane direction. At last, the deflection was so large that it split the part of the web in compression with the other parts of the wall through a dominating diagonal crack. Integrity of the wall was jeopardized and the wall lost majority of its lateral load capacity, as illustrated in FIGURE. The third failure mechanism observed in TWS was web crush, which was a shear controlled failure mechanism as demonstrated in Figure 5. The concrete crushing occurred initially in the unconfined area. Even though the confined concrete in the boundary element did not crush, it could not resist the shear force in the damaged section by itself. A horizontal crack formed in the boundary element and the wall lost majority of its lateral load capacity.

The first failure mechanism The second failure mechanism The third failure mechanism

Figure 5. Illustration of the failure mechanism

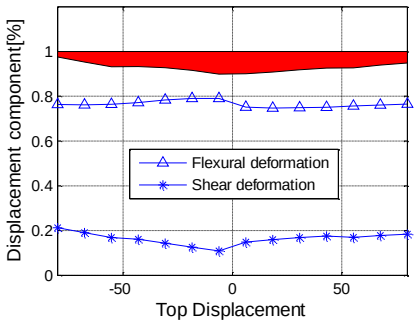

LWS

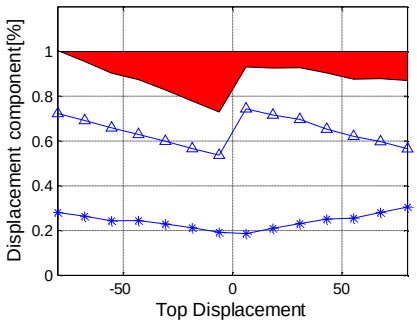

LWN

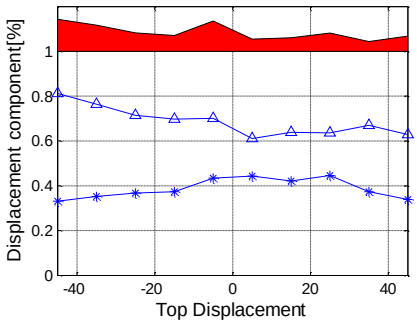

TWS

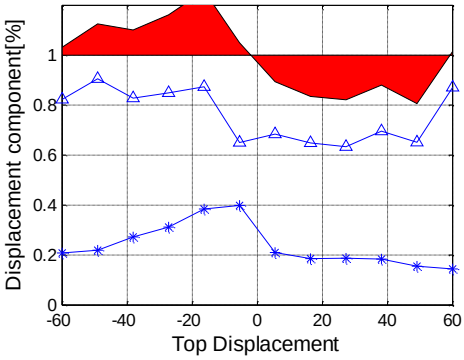

TWN web

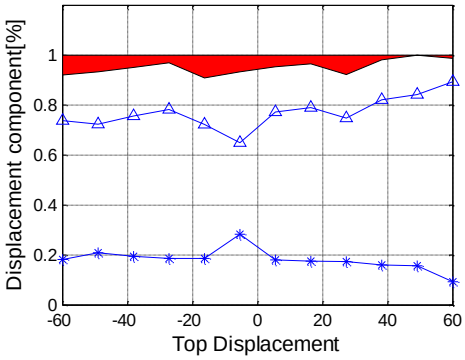

TWN flange

Figure 6. Component of deformation

LVDTs were mounted at different locations of the specimens. Flexural and shear displacements were captured and calculated by the method proposed by Hiraishi[1984]. Figure 6 shows composition of each deformation component for test specimens. The values could not always add up to 100% of the

total displacement which was measured separately. The errors were also reported. As both the flange and the web took part in resisting the shear force in TWN, shear and flexural deformations in these wall segments were both measured and reported seperated in Figure 6.

Strain gauges were attached to various locations of interest in the reinforcement bars. Among them, the most important ones were those monitoring the strain in longitudinal reinforcement at critical sections as these readings are directly related to strength and stiffness of the specimens. The vertical strains detected from these gauges were shown in Figure 7 and Figure 8. The vertical strain profiles were reported at 25%, 50%, 75%, 100% of the expected first yield displacement and the nominal yield displacement. At higher displacement, however, the strains at these locations were often very difficult to detect as the strain gauges often detached from the reinforcement bars at high strain. For LWN, vertical strain in some longitudinal reinforcement bars remained relatively low even at displacements corresponding to maximum lateral load of the specimens due to shear lag effect. In these cases, the attachments of these strain gauges remained intact and the strains at maximum lateral load were also reported.

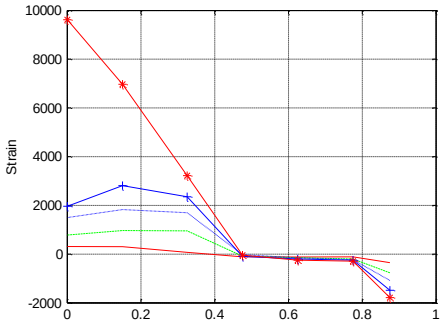

LWS in positive direction

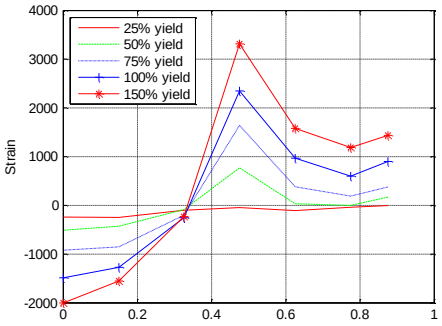

LWS in negative direction

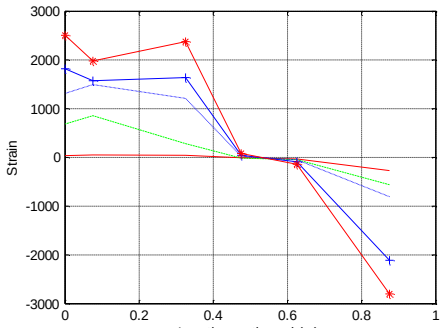

Web of LWN in positive direction

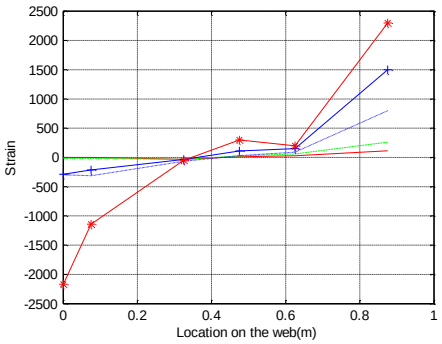

Web of LWN in negative direction

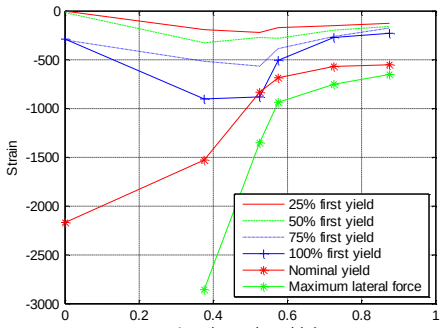

Flange of LWN in positive direction

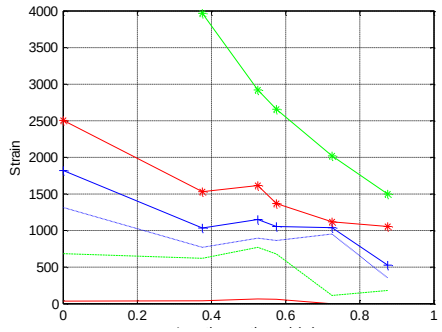

Flange of LWN in negative direction

Figure 7. Section strain profile

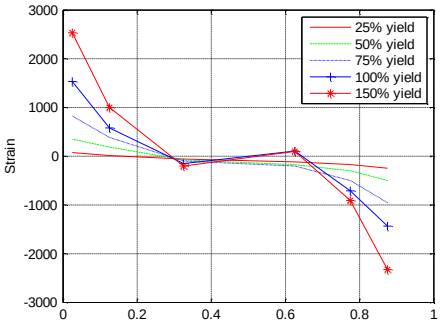

Web of TWS in positive direction

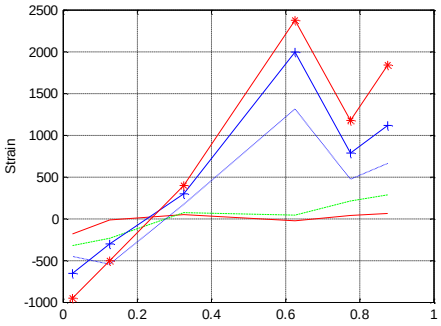

Web TWS in negative direction

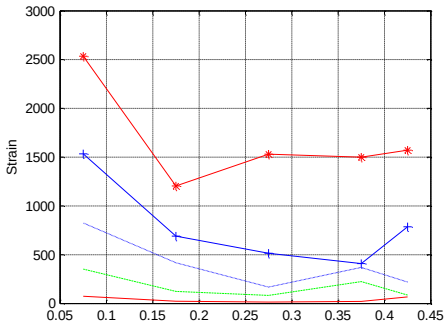

Flange of TWS in positive direction

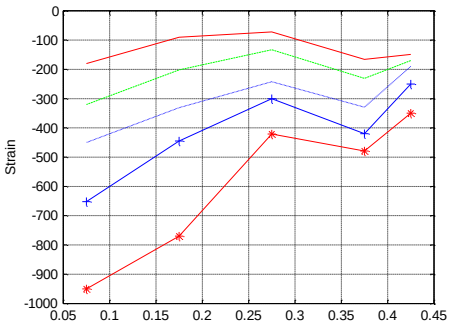

Flange of TWS in negative direction

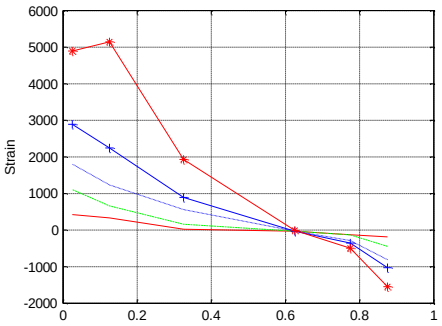

Web of TWN in positive direction

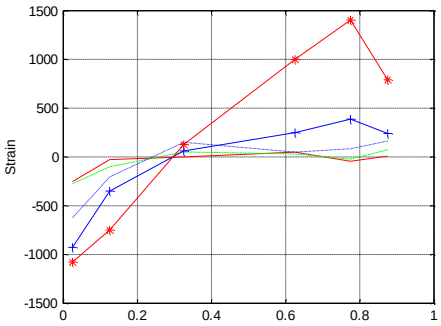

Web of TWN in negative direction

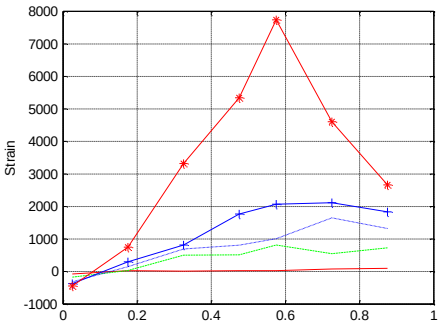

Flange of TWN in positive direction

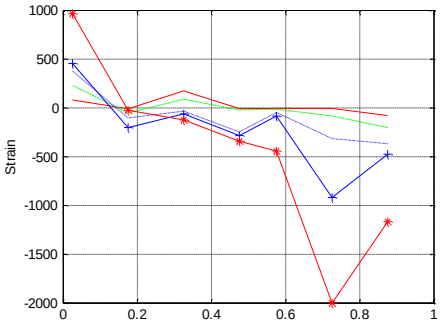

Flange of TWN in negative direction

Figure 8. Section strain profile

Discussions

The test derived hysteresis responses departed from the estimations made by plastic hinge analyses significantly for LWP and TWS. The stiffness of the specimens was overestimated, and the maximum lateral reaction was never reached for certain directions. The overestimation of stiffness is believed to be related to the shear lag effect and shear deformation. Also, both specimens failed before realizing their estimated maximum lateral reactions.

LWN failed due to the loss of stability in the web of the wall. It is worth noting that as the specimen was scaled, some requirements in EC8 [2003] and proposed by Paulay and Priestley [1992] on minimum thickness of the wall boundary elements were not met. Also observed in other tests involving non-rectangular walls [Thomsen Iv and Wallace 2004], this failure mechanism is believed to warrant more attention. In a series of tests which include several other L-shaped specimens loaded in a similar direction as LWN, the out-of-plane deformation which eventually led to buckling of the wall web was always in the same direction. As an unexpected failure mechanism, further investigations are needed.

TWS failed due to web crushing. This is a shear-controlled failure mechanism. This failure mechanism was anticipated as the shear demand of the specimen imposed by the lateral reaction force surpasses the permitted shear force given by the specific requirements for seismic design in ACI318-08 and EC8. These limitations on shear force are believed to be reasonable and precise for ductile structural RC walls even the walls are expected to exhibit moderate ductile behaviour. For structural walls designed in moderate seismic hazard zones which usually possesses higher vertical reinforcement ratios, a diagonal compression failure should be carefully prevented.

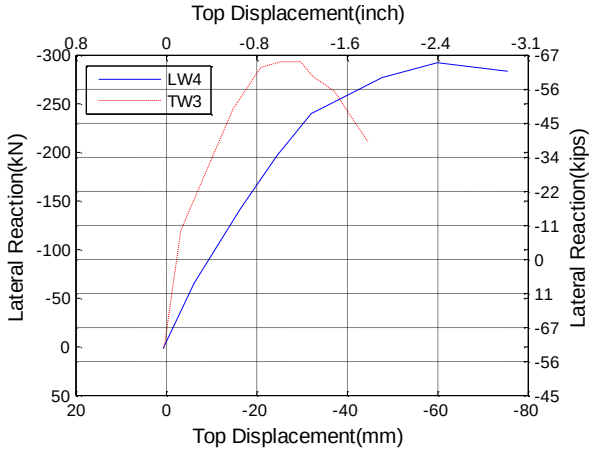

Figure 9. Section strain profile

Table 3. Ratios of the test derived moment at critical section and tension force in the flange to those from section analyses

Maximum flange reinforcement strain	LWN		TWS	
	Moment	Tension force	Moment	Tension force
500	0.51	0.03	0.47	0.40
1000	0.36	0.25	0.60	0.47
1500	0.31	0.38	0.64	0.50
2000	0.37	0.59	0.69	0.76
3000	0.57	0.57	0.74	0.81
4000	0.68	0.62	0.84	0.94

Shear lag effect was found to be of great significance in influencing the behaviour of the specimens. Due to omission of the effect, stiffness of LWN and TWS were severely overestimated. Specifically, this effect has led to a significant difference between the lateral deformation-reaction curve of LWN and of TWS even though these two specimens had almost similar vertical reinforcement in their flanges, as demonstrated in Figure 9. Table 3 summarizes the ratios of test

derived moment at the critical section to the anticipated moment estimated by the nonlinear section analyses corresponding to different maximum reinforcement tension strain. Also calculated and listed in the table are the ratios of the test derived tension force in the flange to the anticipated tension force in the flange based on nonlinear section analyses. As the table shows, both LWN and TWS have demonstrated certain degree of shear lag effect. Also, the influences of the shear lag effect was reduced in both specimens as maximum reinforcement tension strain in the flange increased. The influences of the shear lag effect in LWN were more significant than that of TWS. This difference can be explained by the difference in the geometries of sections of the specimens. The flange of LWN was longer than that of TWS and more main longitudinal reinforcement bars in LWN were gathered in the flange tip away from the web compared to TWS. Compared with the effective flange width specified by ACI 318-11 [2011] and EC8 [2003], the influences of the shear lag effect in TWS was still more significant than what the codes have implied, as its flange should be fully effective taking the effective flange to be one quarter of the wall height. On the other hand, if only the reinforcement in the effective flange width are considered in the nonlinear section analyses of LWN, the expected moment and tension force are 38% and 40% of the test derived values when maximum reinforcement tension strain in the flange reaches the yielding strain. These two ratios were lower than the test derived ratios, indicating that the actual flange effective was longer than expected in LWN. Therefore, it is clear that current defination of the effective flange width is inaccurate for the tested specimens. More research efforts are needed to derive a refined method for consideration of the shear lag effect.

Analyzing the deformation, it was found that the shear deformation contributed a significant ratio to the total deformation. Analyzing the deformation, it was found that shear deformation contributed a significant ratio to the total deformation. The ratio was in general constant during all the loading stages yet different for different loading directions and axial load ratios. The largest value, 39%, was observed in TWS when the flange was in tension. The shear deformation was also quite significant for LWN when the flange was in compression. Given the magnitude of the shear deformation, explicit considerations are needed for predicting the lateral load carrying capacity.

CONCLUSIONS

This paper presented experimental results, analysis and discussions regarding four slender reinforced concrete walls with L-shaped and T-shaped sections under simulated gravity and seismic loads. The following conclusions are drawn:

1. With limited additional confinement, good ductile behaviour can be achieved for non-rectangular walls in various loading directions. However, premature failure mechanisms such as web crushing should be avoided.
2. The test results matched the estimations made by FE analyses well. However, using section analyses together with plastic hinge analyses, the stiffness and maximum reaction force were significantly overestimated for LWN and TWS. Shear lag effect, shear deformation and the web crushing failure mechanism in TWS were believed to be responsible for the overestimation.
3. The three failure mechanisms observed in the test were crushing of concrete in boundary element, loss of stability in the compression web and web crushing. The last failure mechanism was a shear controlled failure mechanism.
4. The shear lag effect showed a significant effect on tension force in the flange. Due to this effect, stiffness of LWN and TWS varied dramatically even these specimens have almost similar vertical reinforcement areas in their flanges. Also, some of the longitudinal reinforcement did not yield even after these specimens lose majority of their lateral load capacity. Consideration of the shear lag effect is needed for preciously predict behaviour of these specimens.
5. The shear deformation accounted for a significant ratio of the total deformation. The ratio of shear deformation to total deformation remained relatively constant during the whole loading process. The maximum ratio was around 45% which was observed in TWN while the flange was in tension.

REFERENCES

ACI (2011). Building Code Requirements for Structural Concrete (ACI 318-11) and Commentary, American Concrete Institude.

Beyer, K., A. Dazio, et al. (2008). "Quasi-static cyclic tests of two U-shaped reinforced concrete walls." *Journal of Earthquake Engineering* 12(7): 1023-1053.

Brueggen, B. L. (2009). Performance of T-shaped Reinforced Concrete Structural Walls under Multi-Directional Loading. Ph.D. Thesis THE UNIVERSITY OF MINNESOTA

CEN (2003). Eurocode 8: Design provisions for earthquake resistance of structures. Brussels, Belgium, European Committee for Standardization. Final Draft prEN 1998–1.

Hiraishi, H. (1984). "Evaluation of Shear and Flexural Deformations of Flexural Type Shear Walls." *Bulletin of the New Zealand Society for Earthquake Engineering* 17(2): 35-144.

Paulay, T. and M. J. N. Priestley (1992). Seismic Design of Reinforced Concrete and Masonry Buildings, John Wiley & Sons, Inc.

Thomsen Iv, J. H. and J. W. Wallace (2004). "Displacement-based design of slender reinforced concrete structural walls - Experimental verification." *Journal of Structural Engineering* 130(4): 618-630.